Molecular path control in zeolite membranes

D. Dubbeldam*†‡, E. Beerdsen*†, S. Calero§, and B. Smit*†

*Centre Européen de Calcul Atomique et Moleculaire, Ecole Normale Supérieure, 46 Allée d'Italie, 69007 Lyon, France; §Department of Experimental Sciences, University Pablo de Olavide, Ctra. Utrera km 1, 41013 Sevilla, Spain; and †Van't Hoff Institute for Molecular Sciences, University of Amsterdam, Nieuwe Achtergracht 166, 1018 WV, Amsterdam, The Netherlands

Edited by David Chandler, University of California, Berkeley, CA, and approved July 14, 2005 (received for review May 12, 2005)

We report molecular simulations of diffusion in confinement showing a phenomenon that we denote as molecular path control (MPC); depending on loading, molecules follow a preferred pathway. MPC raises the important question to which extent the loading may affect the molecular trajectories in nanoporous materials. Through MPC one is able to manually adjust the ratio of the diffusivities through different types of pores, and as an application one can direct the flow of diffusing particles in membranes forward or sideward by simply adjusting the pressure, without the need for mechanical parts like valves. We show that the key ingredient of MPC is the anisotropic nature of the nanoporous material that results in a complex interplay between different diffusion paths as a function of loading. These paths may be controlled by changing the loading, either through a change in pressure or temperature.

anomalous diffusion | nanoporous materials | statistical physics

Among other emerging membrane technologies like polymer-inorganic composites, carbon films, and micro- and mesoporous silica films, zeolite membranes offer outstanding potential for molecular recognition at the subnanometer level and the ability to operate at high temperatures (1, 2). Zeolites are crystalline structures made up of "T-atoms," where T is an aluminum or silicon atom, which are tetrahedrally bonded to each other with oxygen bridges. Because of the regularity of the crystalline structure and the pores with angstrom-size dimensions, these crystals, when grown together to form a membrane, can operate as separation devices for gas and liquid mixtures. From a scientific point of view zeolites are ideal systems to study the effect of confinement on the properties of the adsorbed molecules.

Transport of adsorbates in nanoporous adsorbents such as zeolites is determined by a complex interplay between adsorbent–adsorbate and adsorbate–adsorbate interactions. Molecules diffuse through the pores via various diffusion mechanisms (3). Although interesting effects like single-file diffusion (4), incommensurate diffusion (5, 6), and levitation effects (7) are well known, most of the effects of confinement on diffusion remain poorly understood. This is particularly true for loading effects in materials with different channels and/or cages in the x, y, and z direction. Anisotropic single-component diffusion in silicalite has been known for a long time (8–12). In general, the diffusion coefficients in the different directions can have different dependencies on temperature and loading. A limited number of studies deal with nonzero loading. Bussai *et al.* (13) found little change in anisotropy for water in silicalite as a function of loading. In this article, we report a reversal of anisotropy, i.e., at low loading the diffusivity in the z direction is two times *faster* than in the xy direction for both the self and collective diffusivity, whereas for higher loadings this changes into a z diffusivity that is more than two times *slower*. This behavior is due to a complete change in the diffusion mechanism. Our results raise the unanswered question to which extent the loading may affect the molecular trajectories in nanoporous materials. Here, we focus on what we have named molecular path control (MPC), where one and the same molecular species follows different pathways, depending on the loading. As a specific MPC example, we study the mechanism behind *tunable* anisotropy of ethane in ERI-type zeolite membranes, but the concepts are by no means limited to zeolite materials.

Model and Computational Details

In our simulations, we neglect cations and study rigid, all-silica versions of the ERI- and CHA-type zeolites. Zeolites are designated by three capital letter codes derived from the names of the type materials, e.g., ERI (erionite), and CHA (chabazite). The positions of the atoms are taken from refs. 14 and 15, respectively. Following the work of Bezus *et al.* (16), the zeolites are modeled as a rigid network of oxygen atoms. This is a very common approximation because the large oxygen atoms essentially shield the much smaller silicon atoms, and lattice flexibility is not important for small alkanes in all-silica zeolites (17). The rectangular simulation box sizes we used are $4.5906 \times 3.9756 \times 4.443$ nm for ERI-type zeolite and $3.015 \times 4.7814 \times 2.7606$ nm for CHA-type zeolite. Tests on larger systems did not show any significant finite-size effects. Periodic boundary conditions were used. Adsorption in cation-free structures takes place at sites with little or no electric field. For these reasons the united atom model (18) is a straightforward choice. We consider the CH_3 groups as single, chargeless interaction centers with their own effective potentials. The beads of ethane are connected by a harmonic bonding potential $U^{\text{bond}} = \frac{1}{2}k_1(r - r_0)^2$, with $k_1/k_B = 96{,}500$ K/Å^2 and $r_0 = 1.54$ Å. The non-intramolecular energy is described with a Lennard–Jones potential by using parameters $\sigma_{O-CH_3} = 3.17$ Å, $\varepsilon_{O-CH_3}/k_B = 142$ K, $\sigma_{Si-CH_3} = 2.12$ Å, $\varepsilon_{Si-CH_3}/k_B = 82$ K, and $\sigma_{CH_3-CH_3} = 3.78$ Å, $\varepsilon_{CH_3-CH_3}/k_B = 104$ K, which were taken from ref. 19. The accuracy of the simulation techniques have been verified in several publications (6, 20–23) in which comparisons were made with experimental data and can be considered state-of-the-art for computing adsorption and diffusivities in nanoporous materials.

The simulations were performed by using two different methods: conventional molecular dynamics (MD) and the recently proposed dynamically corrected transition state theory (dcTST) (24, 25). In MD simulations (26–28), successive configurations of the system are generated by integrating Newton's laws of motion, which then yields a trajectory that describes the positions, velocities, and accelerations of the particles as they vary with time. We used the velocity Verlet integration scheme with a time step of 0.5 fs. The relative energy drift was smaller than 10^{-4}. For temperature control we used the Nosé–Hoover chain (NHC) method as formulated by Martyna *et al.* (29). Molecules were inserted into the framework at random positions as long as no overlaps occurred with the framework or other particles. During the initialization period, we performed an NVT (constant number of particles N, volume V, and temperature T) Monte Carlo simulation to rapidly achieve an equilibrium molecular arrangement. After the initialization period, we assigned

This paper was submitted directly (Track II) to the PNAS office.

Abbreviations: CHA, chabazite; dcTST, dynamically corrected transition state theory; ERI, erionite; MD, molecular dynamics.

‡To whom correspondence should be addressed. E-mail: dubbelda@science.uva.nl.

velocities from the Maxwell–Boltzmann distribution at the desired average temperature to all of the atoms. The total momentum of the system was set to zero. Next, we equilibrated the system further by performing an NVT MD simulation using the NHC thermostat. After the equilibration was completed, during the production run of more than 20 ns, we collected statistics using the NVT ensemble. Simulations using the NVE ensemble gave equivalent results. More details can be found in ref. 25.

Although MD and dcTST give equivalent diffusivity results for these systems, dcTST is also applicable in the regime of very slow diffusion, where MD cannot be used, and the behavior is better understood by analyzing the free energy profiles and lattice information provided by the dcTST method. In the dcTST formalism, the diffusion mechanism is divided in two parts. The first is a static term, corresponding to locations of preferable adsorption sites and the free energy barriers in between, the second term generally decreases with loading and corresponds to the inverse of the collision frequency. As such, the dcTST method is able to explain different diffusion regimes over loading, and provides insight into the mechanisms behind an increase or decrease in diffusivity with loading (24).

Using the dcTST method of Beerdsen *et al.* (24, 25), the self-diffusivity is calculated directly by computing the hopping rate of a molecule over a typical length scale λ given by the smallest repeating zeolite structure. The transmission rates are easily converted to diffusion coefficients once the lattice distances and connectivities are known. In ERI-type lattices, shown in Fig. 3, diffusion in the *xy* plane occurs isotropically on a hexagonal lattice

$$D_{xy} = \frac{1}{4} k_{xy} \lambda_{xy}^2, \qquad [1]$$

where λ_{xy} is the lattice displacement distance, and k_{xy} is the corresponding hopping rate. In ERI-type zeolite, each hop in the *z* direction is preceded by a hop in *xy* direction, and diffusion is anisotropic:

$$D_z = \frac{1}{2} \frac{k_{xy} k_z}{k_{xy} + k_z} \lambda_z^2. \qquad [2]$$

Using MD, the self-diffusion coefficients D_S^α in the direction $\alpha = x,y,z$ are computed by taking the slope of the mean-squared displacement at long times

$$D_S^\alpha = \frac{1}{2N} \lim_{t\to\infty} \frac{d}{dt} \left\langle \sum_{i=1}^{N} (r_{i\alpha}(t) - r_{i\alpha}(0))^2 \right\rangle, \qquad [3]$$

where N is the number of molecules, t the time, and $r_{i\alpha}$ the α-component of the center-of-mass of molecule i. The collective diffusion coefficients D_C^α are calculated from

$$D_C^\alpha = \frac{1}{2N\xi} \lim_{t\to\infty} \frac{d}{dt} \left\langle \left(\sum_{i=1}^{N} (r_{i\alpha}(t) - r_{i\alpha}(0)) \right)^2 \right\rangle, \qquad [4]$$

where the term $1/\xi$ is the so-called thermodynamic factor (related to the compressibility of the system), which can easily be evaluated from the adsorption isotherm (30). Collective diffusivity measures the transport of mass and the decay of density fluctuations in the system, whereas self-diffusion measures the diffusive motion of a single particle (30). The collective diffusivity, D_C, is also known as the transport diffusivity, D_T, defined as the proportionality constant between the macroscopic flux and concentration gradient, and is the quantity of experimental interest. In zeolite literature, sometimes the "corrected" diffusivity is used. This type of diffusivity is obtained from the collective (or transport) diffusion by removal of the thermodynamic factor. The "corrected" diffusivity can directly be related to the mean-square displacement of the collective coordinate $\mathbf{R} = \Sigma_{i=1}^{N} \mathbf{r}_i$ (which is N times the coordinate of the center of mass), in analogy to the self-diffusivity. We note that the thermodynamic factor has no influence on ratio of diffusivities.

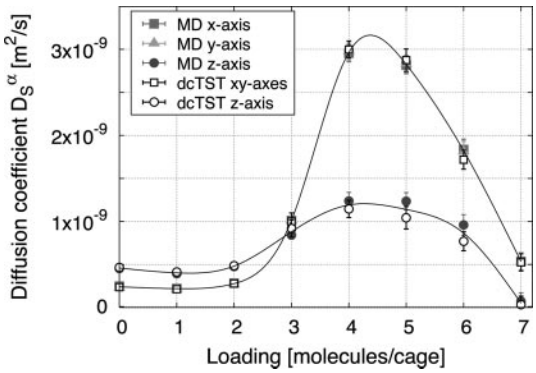

Fig. 1. Anisotropic self-diffusivity D_S^α of ethane in ERI-type zeolite computed by dcTST and conventional MD at 600 K.

Results

In Fig. 1, we have plotted the self-diffusivity of ethane in ERI-type zeolite at 600 K as a function of loading. The ratios D_z/D_{xy} of the self and collective diffusivities are shown in Fig. 2. Very surprisingly, at low loading the diffusivity in the *z* direction is two times *faster* than in the *xy* direction for both the self and collective diffusivity, whereas for higher loadings this changes into a *z* diffusivity that is more than two times *slower*. This behavior directly shows that the molecules follow different pathways when the loading is changed.

The dcTST gives equivalent results to conventional MD. Importantly, the method allows for a more detailed analysis in terms of free energy profiles and transmission coefficients. Eq. **2** shows that diffusion in the *z* direction depends on the hopping rate in both the *z* direction *and* the *xy* direction. An investigation of these hopping rates is made by analyzing the free energy barriers for diffusion in the *xy* plane (Fig. 3). For the diffusion in the *xy* plane, we find "normal" behavior, typical for cage/window-type zeolites (24): The diffusivity increases with loading, because the free energy barrier for diffusion decreases. This behavior is due to the finite volume of a cage, where adding particles to the cage results in more repulsive interactions. In the *z* direction, we find different behavior. Initially, at low loadings, there are no intracage barriers, and therefore the barriers to

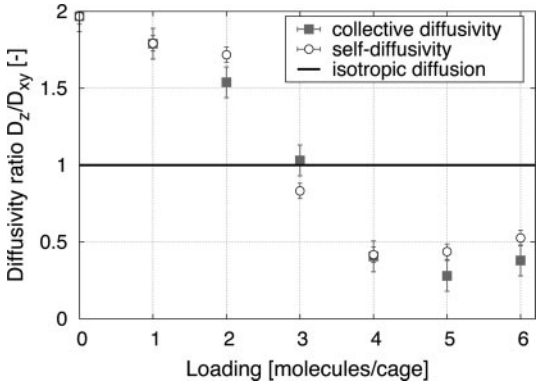

Fig. 2. Anisotropic diffusivity ratio D_z/D_{xy} of ethane in ERI-type zeolite computed by MD at 600 K for self and collective diffusion.

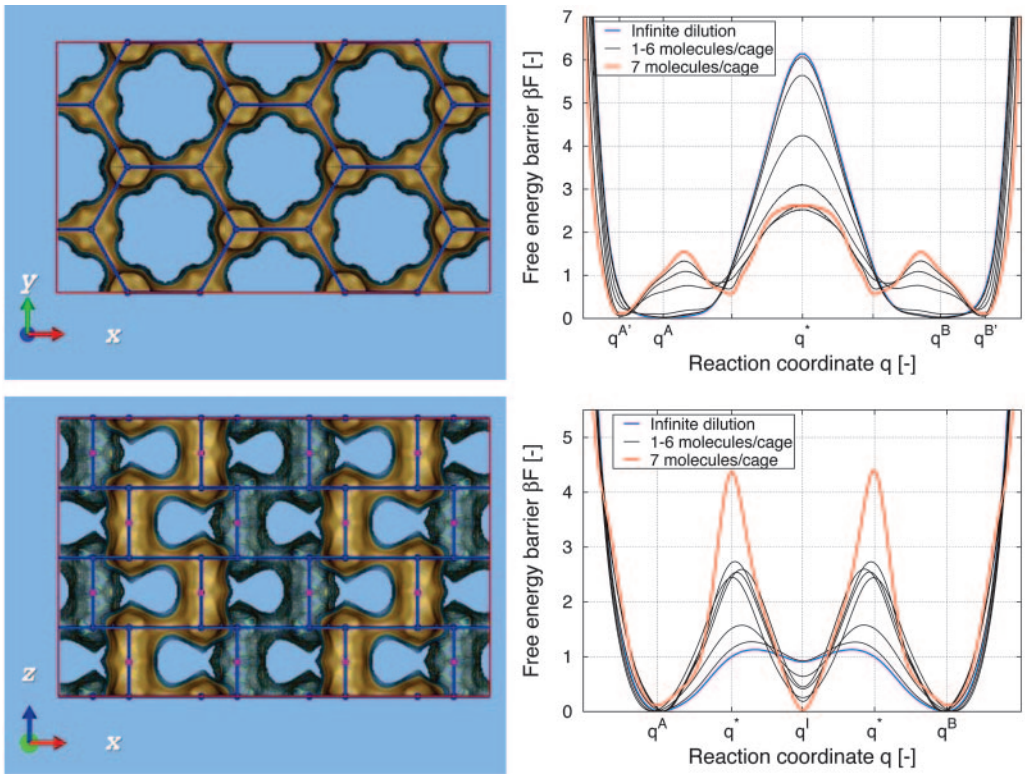

Fig. 3. The ERI-type silica structure crystallizes in the hexagonal dipyramidal space group $P6_3/mmc$ with $a = b = 1.327$ nm, $c = 1.505$ nm, and $\alpha = \beta = 90°$ and $\gamma = 120°$. We show the topology of the ERI-type lattice. (*Upper Left*) In the *xy* direction the hopping takes place on a hexagonal lattice. (*Lower Left*) In the *z* direction a displacement *has* to be preceded first by an *xy* hop. The lattice is drawn in blue dots connected by blue lines of lattice distance $\lambda \approx 0.75$ nm for *x*, *y*, and *z* directions. (*Upper Right*) Free energy profiles $\beta F(q)$ at 600 K of ethane in ERI at various loadings (infinite dilution, 1, 2, 3, 4, 5, 6, and 7 molecules per ERI-type cage) in the hexagonal *xy* plane with q^A the center of a cage, and q^B the center of a neighboring cage. (*Lower Right*) In the *z* direction across a cage with q^A the top of the cage, q^I the middle of the cage, and q^B the bottom of the cage.

diffusion are formed by the *xy* barriers, i.e., the eight-ring windows between the adjacent cages. At higher loadings, the *xy* barriers decrease and new barriers are formed at the centers of the cages. Eventually, the barriers at the centers of the cages dominate the diffusion mechanism, thereby reversing the anisotropy of the diffusion.

It is interesting to note that when the elongation of the erionite cages is removed, i.e., in CHA-type zeolites (Fig. 4), no significant anisotropy is observed in our simulations (Fig. 5). We note that the lattice is only slightly distorted from a cubic lattice and due to symmetry reasons the free energy profiles are all equivalent, i.e., there is only one hopping rate *k* from a cage to *any* of the neighboring cages in CHA-type zeolites. The orientationally averaged diffusion coefficient is *not* affected in CHA-type

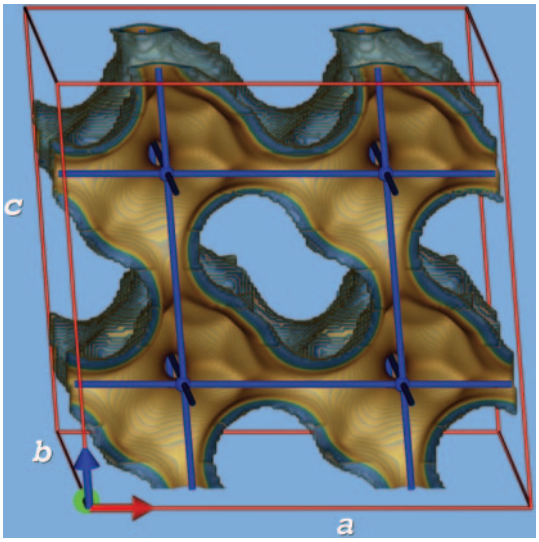

Fig. 4. The CHA-type structure (15) has the space group $R\bar{3}m$ (a squashed cube) with $a = b = c = 0.9459$ nm and $\alpha = \beta = \gamma = 94.07°$. The topology of the CHA-type lattice is shown, where the lattice is drawn in blue dots connected by blue lines.

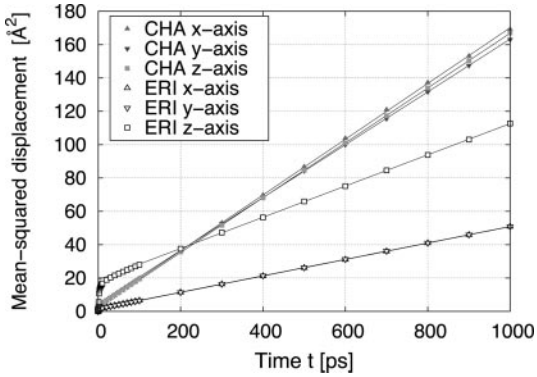

Fig. 5. Mean-squared displacements of self-diffusivity of ethane in CHA- and ERI-type zeolite at 600 K. The diffusion coefficients in the direction $\alpha = x,y,z$ are computed by taking the slope of the mean-squared displacements at long times.

lattices by the distortion effect, but the individual components are, although the effect for 94.07° compared with 90° is negligibly small (<2%). Therefore, diffusion in CHA-type zeolite can be considered isotropic in practice. Also experimentally, tracer diffusion measurements in natural chabazite by Raman spectroscopy did not indicate any substantial deviation from isotropic diffusion (31). However, using the pulsed field gradient NMR technique, Bär *et al.* (32) reported an orientation-dependent diffusivity with a ratio between the maximum and minimum diffusivity of a factor of two, also for water in natural chabazite.

Discussion

We stress that the concept of molecular traffic control (MTC) (33) is different from our molecular path control. It is thought that the origin of MTC lies in the mutual correlation in the movement of a multicomponent fluid through two types of pores (34). MTC has never been convincingly established and has remained a controversial subject for over two decades now, although recently some theoretical progress has been achieved (35–37). The current work demonstrates only how the diffusivity of *one* component may vary between pore systems in the same zeolite. The concept of MTC requires various molecules (reactants and products) to exhibit preferences for different pore systems. However, our results show that these preferences might not only be due to shape-selectivity but also to (local) differences in loading. Moreover, the fact that a *single* component can be tuned to show a preference of one type of pore over another and that this preference can be manually adjusted might be considered even more surprising. This controllability implies the ability of directing adsorbates at the molecular level.

MPC originates from the anisotropic nature of the nanoporous material, e.g., the presence of different channel types or elongated cages. Our results suggest that it is possible to actively design and screen for zeolites with molecular path control properties. As an example, we reported the diffusion of ethane in an erionite-type structure with different diffusion paths, which may be controlled by changing the loading or pressure and temperature. However, the phenomenon is general and by no means limited to zeolites. We have shown that the crucial ingredient is the asymmetric nature of a structure that can be exploited, even for a single component fluid, by using appropriate operating conditions.

We thank T. J. H. Vlugt for comments on the manuscript. This work was supported by the Netherlands Research Council, Deutsche Forschungsgemeinschaft Priority Program SPP 1155, Spanish Ministry of Science and Technology Ramón y Cajal Program and Grant VEM2003 20574 C03 01, and the European Commission. The Netherlands Organization for Scientific Research/National Computer Facilities provided computational resources.

1. Davis, M. E. (2003) *Science* **300,** 438–439.
2. Lai, Z., Bonilla, G., Diaz, I., Nery, J. G., Sujaoti, K., Amat, M. A., Kokkoli, E., Terasaki, O., Thompson, R. W., Tsapatsis, M. & Vlachos, D. G. (2003) *Science* **300,** 456–460.
3. Kärger, J. & Ruthven, D. M. (1992) *Diffusion in Zeolites and Other Microporous Solids* (Wiley, New York).
4. Hahn, K., Kärger, J. & Kukla, V. (1996) *Phys. Rev. Lett.* **76,** 2762–2765.
5. Gorring, R. L. (1993) *J. Catal.* **31,** 13–26.
6. Dubbeldam, D., Calero, S., Maesen, T. L. M. & Smit, B. (2003) *Phys. Rev. Lett.* **90,** 245901.
7. Ghorai, P. K., Yashonath, S., Demontis, P. & Suffritti, G. B. (2003) *J. Am. Chem. Soc.* **125,** 7116–7123.
8. June, R. L., Bell, A. T. & Theodorou, D. N. (1990) *J. Phys. Chem.* **94,** 8232–8240.
9. Kärger, J. (1991) *J. Phys. Chem.* **95,** 5558–5560.
10. Hong, U., Kärger, J., Kramer, R., Pfeifer, H., Seiffert, G., Muller, U., Unger, K. K., Luck, H. B. & Ito, T. (1991) *Zeolites* **11,** 816–821.
11. June, R. L., Bell, A. T. & Theodorou, D. N. (1992) *J. Phys. Chem.* **96,** 1051–1060.
12. Maginn, E. J., Bell, A. T. & Theodorou, D. N. (1996) *J. Phys. Chem.* **100,** 7155–7173.
13. Bussai, C., Fritzsche, S., Haberlandt, R. & Hannongbua, S. (2003) *J. Phys. Chem. B.* **107,** 12444–12450.
14. Gard, J. A. & Tait, J. M. (1973) *Proceedings of the Third International Conference on Molecular Sieves*, ed. Uytterhoeven, J. B. (Leuven Univ. Press, Zurich), pp. 94–99.
15. Calligaris, M., Nardin, G. & Randaccio, L. (1983) *Zeolites* **3,** 205–208.
16. Bezus, A. G., Kiselev, A. V., Lopatkin, A. A. & Du, P. Q. J. (1978) *J. Chem. Soc. Faraday Trans. 2* **74,** 367–379.
17. Vlugt, T. J. H. & Schenk, M. (2002) *J. Phys. Chem. B* **106,** 12757–12763.
18. Ryckaert, J. P. & Bellemans, A. (1978) *Faraday Dicuss. Chem. Soc.* **66,** 95–106.
19. Schüring, A., Auerbach, S. M., Fritzsche, S. & Haberlandt, R. (2002) *J. Chem. Phys* **116,** 10890–10894.
20. Calero, S., Dubbeldam, D., Krishna, R., Smit, B., Vlugt, T. J. H., Denayer, J. F. M., Martens, J. A. & Maesen, T. L. M. (2004) *J. Am. Chem. Soc.* **126,** 11377–11386.
21. Dubbeldam, D., Calero, S., Vlugt, T. J. H., Krishna, R., Maesen, T. L. M., Beerdsen, E. & Smit, B. (2004) *Phys. Rev. Lett.* **93,** 088302.
22. Dubbeldam, D., Calero, S., Vlugt, T. J. H., Krishna, R., Maesen, T. L. M. & Smit, B. (2004) *J. Phys. Chem. B* **108,** 12301–12313.
23. Vlugt, T. J. H., Krishna, R. & Smit, B. (1999) *J. Phys. Chem. B* **103,** 1102–1118.
24. Beerdsen, E., Smit, B. & Dubbeldam, D. (2004) *Phys. Rev. Lett.* **93,** 248301.
25. Dubbeldam, D., Beerdsen, E., Vlugt, T. J. H. & Smit, B. (2005) *J. Chem. Phys.* **122,** 224712.
26. Allen, M. P. & Tildesley, D. J. (1987) *Computer Simulation of Liquids* (Clarendon, Oxford).
27. Rapaport, D. C. (2004) *The Art of Molecular Dynamics Simulation* (Cambridge Univ. Press, Cambridge, U.K.), 2nd Ed.
28. Frenkel, D. & Smit, B. (2002) *Understanding Molecular Simulation* (Academic, London), 2nd Ed.
29. Martyna, G. J., Tuckerman, M. E., Tobias, D. J. & Klein, M. L. (1996) *Mol. Phys.* **87,** 1117–1157.
30. Ala-Nissila, T., Ferrando, R. & Ying, S. C. (2002) *Adv. Phys.* **51,** 949–1078.
31. Goryainov, S. V. & Belitsky, I. A. (1995) *Phys. Chem. Miner.* **22,** 433–452.
32. Bär, N.-K., Kärger, J., Pfeifer, H., Schäfer, H. & Schmitz, W. (1998) *Microporous Mesoporous Mater.* **22,** 289–295.
33. Derouane, E. G. & Gabelica, Z. (1980) *J. Catal.* **65,** 486–489.
34. Clark, L. A., Ye, G. T. & Snurr, R. Q. (2000) *Phys. Rev. Lett.* **84,** 2893–2896.
35. Bräuer, P., Brzank, A. & Kärger, J. (2003) *J. Phys. Chem. B* **107,** 1821–1831.
36. Neugebauer, N., Bräuer, P. & Kärger, J. (2000) *J. Catal.* **194,** 1–3.
37. Bräuer, P., Neugebauer, N. & Kärger, J. (2001) *Colloids Surf.* **187–188,** 459–467.